Metrology of high-n Rydberg states of molecular hydrogen with $\Delta\nu/\nu = 2 \times 10^{-10}$ accuracy

Maximilian Beyer, Nicolas Hölsch, Josef A. Agner, Johannes Deiglmayr, Hansjürg Schmutz, and Frédéric Merkt
Laboratorium für Physikalische Chemie, ETH Zürich, 8093 Zürich, Switzerland

(Received 24 November 2017; published 3 January 2018)

Precision spectroscopy of molecular Rydberg states of high principal quantum number ($n \geqslant 50$) followed by Rydberg series extrapolation currently represents the most accurate method of determining the ionization energies of neutral molecules. Until recently, such determinations relied on the use of pulsed laser radiation and supersonic molecular beams, which limited the spectral linewidths and induced ac Stark shifts, thus causing undesirable statistical and systematic uncertainties. We report on the combination of single-mode continuous-wave laser radiation, calibrated with a frequency comb, with slow supersonic beams expanding from low-temperature reservoirs, to record transitions to high-n molecular Rydberg states with unprecedented accuracy. As illustration, we present the result of a measurement, with a relative frequency accuracy of $\Delta\nu/\nu = 2 \times 10^{-10}$ and an absolute accuracy of 64 kHz, of the transition from the $GK\ ^1\Sigma_g^+(v = 0, N = 2)$ state of H_2 to the $n = 50$ f Rydberg state belonging to a series converging on the $X^+\ ^2\Sigma_g^+(v^+ = 0, N^+ = 0)$ ground state of H_2^+. The accuracy of the result [$\nu_{\rm NIR} = 380\,132\,832.236(0.035)_{\rm stat}(0.054)_{\rm sys}$MHz] approaches the accuracy that can be achieved in similar measurements on ultracold alkali-metal-atom samples, although the dominant sources of uncertainties are different. The implications of our result for precision measurements of the adiabatic ionization energy of H_2 and of the energy-level structure of H_2^+ are discussed.

DOI: 10.1103/PhysRevA.97.012501

I. INTRODUCTION

Precision measurements of the energy intervals between the quantum states of molecules represent one of the main tasks of high-resolution spectroscopy and enables one to derive information on molecular structure and dynamics. Precision measurements in few-electron molecules additionally provide the opportunity to test the results of *ab initio* calculations that include relativistic and QED effects [1–5]. The ultimate goals of such tests are to check the theoretical results within their expected accuracy, which ideally would be limited by the uncertainties of the fundamental constants, or to detect significant discrepancies between experimental and theoretical results. In the former case, precision measurements offer a route to improved values of the fundamental constants used to relate computational and experimental results. In the latter, they provide an incentive and a justification for extending the theoretical framework by considering "new" effects. The comparison of precision measurements and *ab initio* calculations of energy intervals in the hydrogen atom and muonic hydrogen has given rise to what is known as the proton-charge-radius puzzle (see, e.g., [6,7]), which is in essence an incompatibility of results at the level of 4.5% [0.84087(39) fm vs 0.8779(94) fm] that would require a change of the Rydberg constant by several standard deviations from the value given by CODATA2014 [8].

Precision determinations of energy intervals in molecules, though more challenging both experimentally and theoretically, may provide information not available from studies of atoms. In this context, the one- and two-electron molecules H_2^+ and H_2 are particularly attractive because their energy levels can be calculated with extraordinary accuracy [3,5]. For instance, the effect of the finite size of the proton on the dissociation energy D_0 of H_2 is calculated to be 0.000 031 cm^{-1}, or 930 kHz [2], so that a 4.5% change of the value of the proton radius would change the value of the dissociation energy by 1.4×10^{-6} cm^{-1} (42 kHz), a value that is not out of reach of modern spectroscopic experiments on H_2 [9,10].

Current experimental efforts at improving the dissociation energy of H_2 rely on the determination of the adiabatic ionization energy of H_2 [current value of 124 417.491 13(37) cm^{-1} [11]] as sums of several energy intervals, such as [11]

$$X(v'' = 0, N'' = 0) - EF(v', N');\quad EF(v', N') - \text{high } n;\quad \text{high } n - X^+(v^+ = 0, N^+ = 0) \tag{1}$$

or

$$X(v'' = 0, N'' = 0) - GK(v', N');\quad GK(v', N') - \text{high } n;\quad \text{high } n - X^+(v^+ = 0, N^+ = 0) \tag{2}$$

(see Ref. [10] for a detailed discussion and the determination of the last interval at an accuracy of 50 kHz).

In a previous effort, the $GK(1,1) - 56p1_1$ interval of H_2 was measured to be 378 809 478.7 MHz, with a precision of 1.2 MHz limited in equal parts by the statistical uncertainty associated with the determination of the centers of the Doppler-broadened lines (19 MHz full width at half maximum) and by the systematic uncertainty resulting from the ac Stark shifts caused by the pulsed near-infrared laser radiation [12].

We report here on the following improvements of this measurement that have enabled us to reduce the uncertainty by a factor of more than 10. (i) The pulsed valve used to generate the supersonic beam of H_2 was operated at several temperatures down to 40 K rather than 300 K, which reduced the beam velocity by a factor of up to 3, and the collimation of the supersonic beam was improved, which reduced the Doppler width of the line below 2 MHz. (ii) The ac Stark shift and its

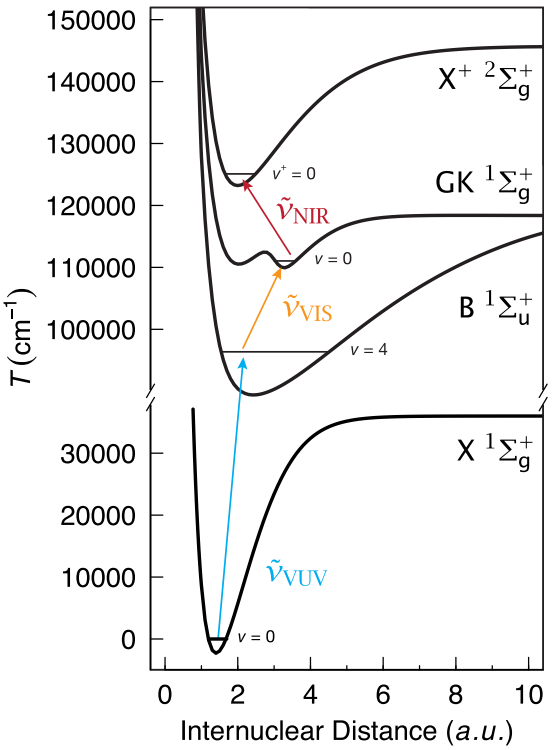

FIG. 1. Excitation scheme to study the transitions from the $GK(0,2)$ state to $nf[X^+(0,0)](S=0)$ Rydberg states (see text for details).

uncertainty were entirely suppressed by replacing the pulsed NIR laser used to record the $GK(v,N)$–high-n interval by a continuous-wave (cw) single-mode laser. (iii) The frequency of this laser was stabilized to a frequency comb, resulting in a laser bandwidth of 1.2 MHz and a frequency-calibration accuracy better than 3 kHz. Finally, (iv) the $GK(0,2)$ state rather than the $GK(1,1)$ state was selected as intermediate level because of its longer lifetime [69(6) ns instead of 24(3) ns [13]]. A measurement in para H_2 also avoids the complications arising from the hyperfine structure and offers a more direct way to determine the adiabatic ionization energy.

The combination of these efforts allowed us to determine the transition frequencies with a relative accuracy of $\Delta\nu/\nu = 2\times10^{-10}$ and an absolute accuracy of 64 kHz, which closely approaches the accuracy of similar measurements in ultracold samples of laser-cooled atoms [14]. The comparison of the main sources of uncertainties affecting the two measurements, presented in the last section of this article, reveals their different origin and indicates possible strategies for their reduction in future experiments.

II. EXPERIMENTAL PROCEDURE

The frequencies of the transitions from the $GK\ ^1\Sigma_g^+(v=0, N=2)$ state of para-H_2 to the singlet $n=50$ f and $n=70$ f Rydberg states belonging to series converging to the $X^+\ ^2\Sigma_g^+(v^+=0, N^+=0)$ ground state of H_2^+ were measured using the following resonant multiphoton excitation scheme (see Fig. 1):

$$n\,f[X^+(0,0)](S=0) \xleftarrow{\text{NIR}} GK(0,2) \xleftarrow{\text{VIS}} B(4,1) \xleftarrow{\text{VUV}} X(0,0). \quad (3)$$

The laser system employed for this sequence and used in this work is depicted schematically in Fig. 2 and consists of pulsed vacuum-ultraviolet (VUV) and visible (VIS) laser systems for the first two steps of the excitation and of a cw single-mode near-infrared (NIR) laser for the final transition. The justifications for using pulsed lasers to prepare the intermediate $GK(0,2)$ state are (i) that the $B-X$ transition lies in the VUV at around $\lambda_{\text{VUV}} \approx 105$ nm [15], a wavelength that is generated by four-wave mixing, which requires high intensities, and (ii) that the short lifetime and associated large natural linewidth of the $B(4,1)$ state [$\tau \approx 0.69(15)$ ns [13]] makes the excitation with cw single-mode radiation extremely inefficient.

The VUV radiation ($\tilde\nu_{\text{VUV}} = 2\tilde\nu_1 + \tilde\nu_2$) was produced by resonance-enhanced four-wave mixing in xenon using two pulsed lasers. The wave number $\tilde\nu_1$ of the first laser was fixed at the position of the $5p^5(^2P_{3/2})6p[1/2](J=0) \leftarrow 5p^6\ ^1S_0$ two-photon transition of Xe ($2\tilde\nu_1 = 80\,118.970\ \text{cm}^{-1}$) and was generated by frequency tripling the output of a commercial Nd:YAG-pumped pulsed dye laser using two successive BBO crystals. The second laser ($\tilde\nu_2 = 15\,176.540\ \text{cm}^{-1}$) used in the four-wave mixing process was a commercial dye laser pumped by the same Nd:YAG laser. The $GK-B$ transition was induced by the visible output ($\tilde\nu_{\text{VIS}} = 16\,398.218\ \text{cm}^{-1}$) of a third commercial dye laser. The timing and optical paths of all three dye lasers were optimized so that the VUV and VIS laser beams overlapped temporally and spatially in the excitation chamber, where they crossed a supersonic beam of H_2 at right angles in the excitation region depicted in Fig. 3 and described below.

The pulse energies of the VUV laser (~1 nJ) were sufficient to saturate the $B-X$ transition whereas the pulse energies of the visible laser were attenuated to about 1 μJ to avoid resonance-enhanced multiphoton ionization of the $GK(0,2)$ state. In addition, care was taken that the beam diameters of the lasers at the excitation spot were about 1 mm to avoid the formation of significant ion concentrations in the excitation volume. This measure also limited the density of Rydberg states produced by the NIR radiation.

A commercial Ti:Sa ring laser [16] pumped by the 10-W output of a diode-pumped, frequency-doubled Nd:YVO_4 laser [17] provided the cw single-mode NIR radiation to drive the $n\,f[X^+(0,0)](S=0) - GK(0,2)$ transitions. The maximal power of the NIR radiation was 1.4 W but only a fraction (typically 20 mW to 1 W) was used for the actual excitation. The 12-m-long path between the ring laser and the excitation spot served the purposes of selecting the TEM_{00} mode and of minimizing systematic errors associated with the first-order Doppler shift, as described below. Two telescopes were used to match the NIR-laser beam size to the sizes of the VUV and VIS laser beams in the excitation region. To stabilize the NIR-laser frequency, a fraction of the ring-laser output (30 mW) was coupled into a polarization-maintaining fiber and overlapped with the output beam of a frequency comb [18] with orthogonal polarization using a fiber-based beam combiner. To measure a

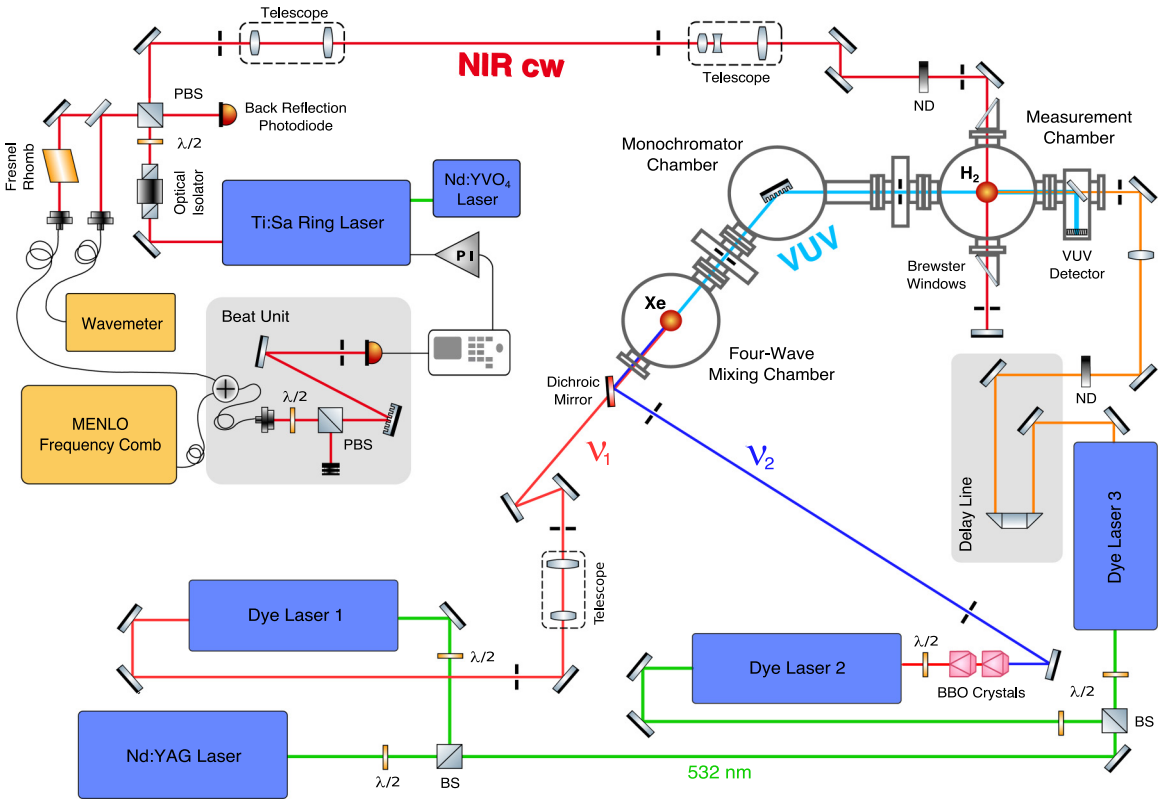

FIG. 2. Schematic overview of the experimental setup (see text for details).

beat-note signal, the overlapped beams traversed a half-wave plate and a polarizing beam splitter which selected the parallel polarization components of both beams. The beat signal was monitored with a fast photodiode connected to a home-built low-noise preamplifier and used to generate an error signal following the procedure described in Ref. [19]. Using an analog proportional-integral (PI) controller, the error signal was fed back to the electronic control unit of the ring laser, which was modified as described in Ref. [20]. The frequency stabilization resulted in a reduction of the linewidth from 5 MHz (limited by the internal reference cavity of the ring laser) to 1.2 MHz, as estimated from the analysis of the beat-note measurements. The frequency of the ring laser was scanned in steps of typically 300 kHz by altering the repetition rate of the frequency comb. To identify the mode number of the comb tooth contributing to the beat-note signal, the ring-laser output frequency was determined with an accuracy of 60 MHz (3σ) with a wave meter [21].

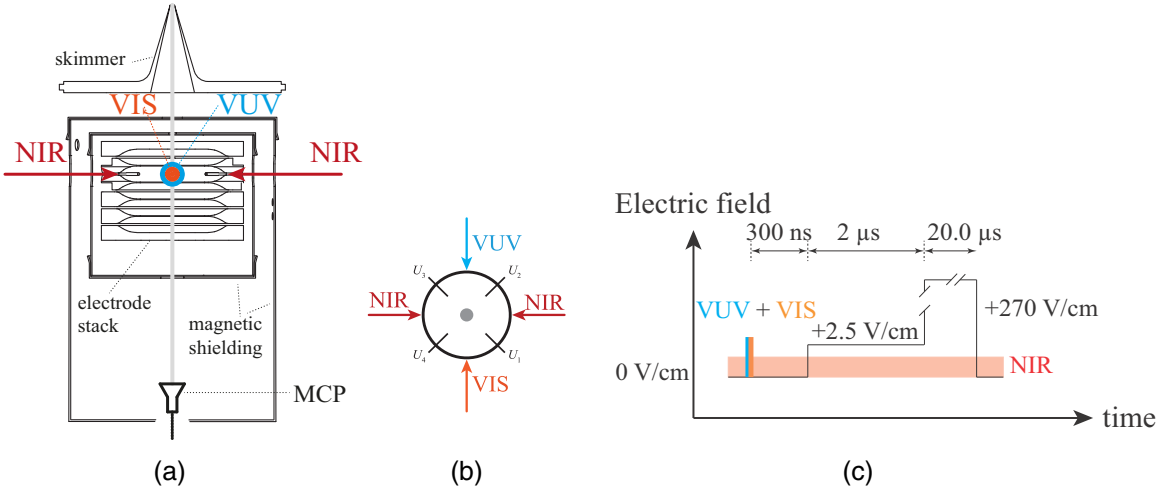

FIG. 3. Measurement chamber and detection sequence. (a) Electrode stack with photoexcitation region, surrounded by a mumetal magnetic shield. The molecular beam (gray line) crosses the laser beams (colored arrows) at right angles. (b) Rod electrodes used for the compensation of stray electric fields in the plane perpendicular to the stack axis. (c) Electric-field pulse sequence used for the pulsed-field ionization of Rydberg states (see text for details).

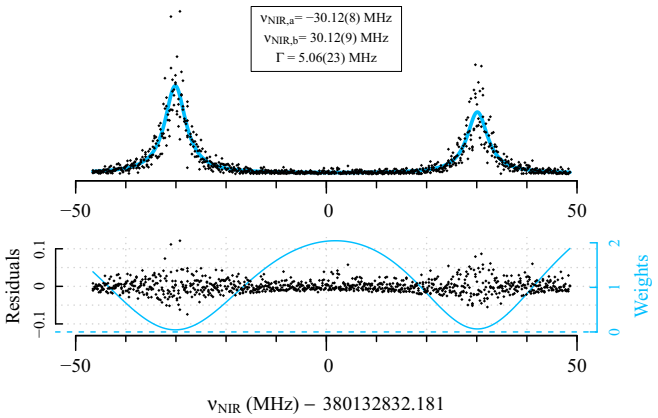

FIG. 4. Spectrum of the $50f0_3 \leftarrow GK(0,2)$ transition with the analysis using a Lorentzian line-shape model. Upper panel: fit of the line model (blue lines) to the raw data (black points). Lower panel: weighted residuals (black points) and relative weights (blue lines) used in the fitting procedure. The fitted line-shape parameters are given in the inset.

All frequencies reported in this article were obtained by direct comparison with the 10-MHz reference frequency of a Rb oscillator [22] having a fractional stability of 2×10^{-11} over a typical measurement time of 1 s (time to acquire one data point) and being disciplined by a GPS receiver [23] with a specified long-term stability of 10^{-12}. This calibration procedure resulted in an absolute frequency uncertainty of less than 3 kHz. The NIR-laser beam was introduced into the chamber through a side port with a window mounted at Brewster's angle to suppress reflection losses. The NIR beam crossed the H_2 beam at ∼90° and exited the chamber through a second Brewster window before impinging onto a 180° reflection mirror. The reflected NIR-laser beam crossed the H_2 sample again and the reflection angle was checked to be $180° \pm 0.003°$ by monitoring the reflected beam at a distance of 12 m from the reflection mirror, thereby ensuring a perfect overlap over the entire beam path. By introducing a small deviation from 90° of the angle between the NIR and the H_2 beam, a small Doppler shift was induced and adjusted in the range 0–(±50) MHz for the forward and reflected beams. Consequently, each transition was observed as two well-separated Doppler components (see Fig. 4). The Doppler-free transition frequency was determined by taking the average of the central frequencies of both components.

The molecular beam was a supersonic beam of pure H_2 generated by a home-built cryogenic valve, described in Ref. [24], but improved by (i) reducing the mass of the plunger by 30% and (ii) encasing the solenoid in a soft magnetic structure [25] to enhance the magnetic field acting on the plunger. In this manner, short pulses (∼30 μs) could be produced at a valve temperature of 88 K and the plunger rebounce observed in Ref. [24] could be fully suppressed. The supersonic beam was collimated using two skimmers, the first (second) with a 12-mm (1-mm) orifice diameter and located 25 cm (75 cm) away from the valve orifice. The beam velocity v_{beam} was about 2700, 1400, and 1000 m/s when the valve body was held at 298, 88, and 40 K, respectively. The velocity component of the molecular beam parallel to the NIR propagation direction was reduced to less than v_{beam} sin [0.5/750] corresponding to a kinetic temperature of ∼100 μK at a valve temperature of 88 K. The Doppler width at $\tilde{\nu}_{NIR} \approx 12\,680\ cm^{-1}$ was thus reduced to ∼3.7, ∼2.0, and ∼1.2 MHz, respectively. The velocity distribution of the molecules along the propagation axis of the molecular beam in the photoexcitation region was determined by monitoring the H_2^+ photoionization signal as a function of the delay between the nozzle opening time and the laser pulse and corresponds to a temperature of ∼1.1 K.

The photoexcitation region is represented schematically in Fig. 3(a). It is enclosed in a double-layer magnetic shield (mumetal) and consists of a set of six cylindrical electrodes with shapes optimized to generate homogeneous field distributions at the excitation spot. The Rydberg states were detected by pulsed-field ionization with a field of ∼270 V/cm and monitoring the H_2^+ ions using a microchannel-plate detector located at the end of a time-of-flight spectrometer. Prompt H_2^+ ions were separated from H_2^+ ions produced by pulsed-field ionization (PFI) by applying a small electric-field pulse (2.5 V/cm) delayed by 300 ns with respect to the VUV and VIS laser pulses, allowing an interaction time of 300 ns of the molecules in the intermediate GK state with the NIR radiation [see Fig. 3(c)]. Because of the long lifetimes of the f Rydberg states (>5 μs), the ionization pulse could be delayed by 2.3 μs to ensure a perfect separation of the prompt and PFI H_2^+ signal along the time-of-flight spectrometer.

The component of the stray electric field along the axis of the electrode stack (typically 3 mV/cm) was compensated by applying a dc potential difference across the stack. Residual fields in the plane perpendicular to the stack axis were compensated by applying electric potentials U_1 to U_4 to the four rod electrodes mounted in the plane, as depicted in Fig. 3(b). Electric stray fields along the VUV propagation direction were caused by charged particles created by the VUV radiation, which is partially reflected at the exit window (corresponding to the entrance port for the visible laser beam) back toward the electrode stack. This effect was reduced by mounting this exit window at an angle of 45°.

III. RESULTS

Spectra of high Rydberg states are particularly sensitive to experimental conditions. To derive not only precise but also accurate line positions, efforts must be invested to determine the line centers, to describe the line shapes, and to study how these are influenced by the experimental conditions. To this end, we varied the experimental parameters and recorded spectra of Rydberg states of different principal quantum number. The estimated uncertainties for the transition to the $50f0_3$ Rydberg state are summarized in Table I.

A. Statistical uncertainties

For a given signal-to-noise ratio, the precision at which a line center can be determined is inversely proportional to the width of the line. Line broadening is a dominant source of statistical uncertainties in the determination of the line positions. The sources of line broadening beyond the natural linewidth relevant to our measurement are Doppler and pressure broadening and the laser bandwidth.

TABLE I. Comparison of the determination of the transition frequencies to Rydberg states of H_2 using a skimmed supersonic beam and of Cs using laser-cooled atoms.

	H_2	Cs
Initial state	$GK\ ^1\Sigma_g^+\ (3s/d)$	$6\,^2S_{1/2}\ (F=4)$
Final state	$50\ f0_3(S=0,v^+=0)^2\Sigma_g^+$	$74p\ ^2P_{3/2}$
$\tilde{\nu}$ (cm^{-1})	12 700	31 250
α_{nl} [MHz/(V/cm)^2]	$5.47(11)\times10^4$	2.3×10^4[a]
Lifetime initial state (ns)	69(6)	$>10^9$
Lifetime final state (μs)	>5	>10
Γ_{natural} (MHz)	2.31(20)	<0.001
Density (particles/cm^3)	10^{11}	6×10^{10}
Sample volume (mm^3)	1	3.4×10^{-3}
Mass (u)	2.0	132.9
Temperature (μK)	100[b]	70
Velocity (m/s)	1390[c]	0
Γ_{laser} (MHz)	1.2	1.0
Γ_{Doppler} (MHz)	<2	0.6
Γ_{FWHM} (MHz)	5	1.4
Electric field (mV/cm)	<0.8	<1
Magnetic field (mG)	≪40	<2
Line-shape model (kHz)	<50	<1
dc Stark shift (kHz)	18	<20
Zeeman shift/broadening (kHz)	<10	<1
ac Stark shift (kHz)	<4	486(16)[d]
Rydberg-Rydberg interaction (kHz)	≪1	<1
Pressure shift (kHz)	<1	∼8
First-order Doppler shift (kHz)	<110[e]	≪1
Second-order Doppler shift (kHz)	4.1(5)	<1
σ_{stat} (kHz)	91	60
σ_{sys} (kHz)	54	25

[a]Calculated using the approach described in Ref. [39].
[b]Corresponds to the width of the velocity distribution in the direction of the NIR laser beam.
[c]For a valve temperature of 88 K.
[d]ac Stark shift caused by residual light from the optical-dipole-trapping laser.
[e]The uncertainty averages out over several measurements and contributes to σ_{stat} (see text).

The lifetimes of the p/f Rydberg states of H_2 belonging to series converging to the $X^+(0,0)$ ground state of para-H_2^+ exceed the lifetime of the $GK(0,2)$ state [$\tau = 69(6)$ ns [13]] by several orders of magnitude and extend until the transitions are detected by pulsed-field ionization of the Rydberg states 2.3 μs after the laser pulses. In the absence of line broadening, the transitions are expected to have Lorentzian line shapes with a linewidth of $\Gamma_{\text{FWHM}} = 2.31(20)$ MHz, corresponding to the natural lifetime of the $GK(0,2)$ state [13]. The 75-cm distance between the valve orifice (diameter 1 mm) and the second skimmer restricts the Doppler width to 3.7, 2.0, and 1.2 MHz for valve temperatures of 298, 88, and 40 K, respectively. The Doppler broadening of the lines depends on the velocity distribution in the volume defined by the spatial overlap of all three laser beams in the excitation region and can deviate from a Gaussian distribution.

Depending on the broadening mechanisms, the measured lines may have Gaussian, Lorentzian, or Voigt line shapes. The laser linewidth (∼1.2 MHz) is not much narrower than the expected natural linewidth. In order not to have to make any assumption concerning the dominant broadening mechanisms, the spectra were analyzed using Lorentzian, Gaussian, and Voigt profiles. However, when fitting Voigt profiles to the observed line shapes, the Gaussian contribution was found to always be significantly narrower than the Lorentzian contribution. After verifying that the line centers and the residuals did not depend on whether we used a Voigt or a Lorentzian profile, the spectra were analyzed using a Lorentzian line-shape model. Because the line profile was found to be symmetric, the exact nature of the line-shape model did not significantly affect the central frequency.

To obtain reliable values for the fit parameters (six parameters for a given transition, i.e., one line center and one amplitude for each of the two Doppler components, one linewidth, and one baseline value) and their uncertainties in the nonlinear fit, the data points were weighted by taking into account the Poissonian nature of the detection method (signal proportional to the number of ions) and the intrinsic noise of the detector electronics [26,27]. The weighting procedure was iteratively refined until the fit procedure converged, at which point we verified that the residuals were normally distributed with a width as independent of the frequency as possible, as depicted in Fig. 4 for the $50\ f0_3 \leftarrow GK(0,2)$ transition recorded under optimized experimental conditions. The same analysis with a Gaussian line-shape model led to a slightly more pronounced frequency dependence of the residuals. The uncertainties of

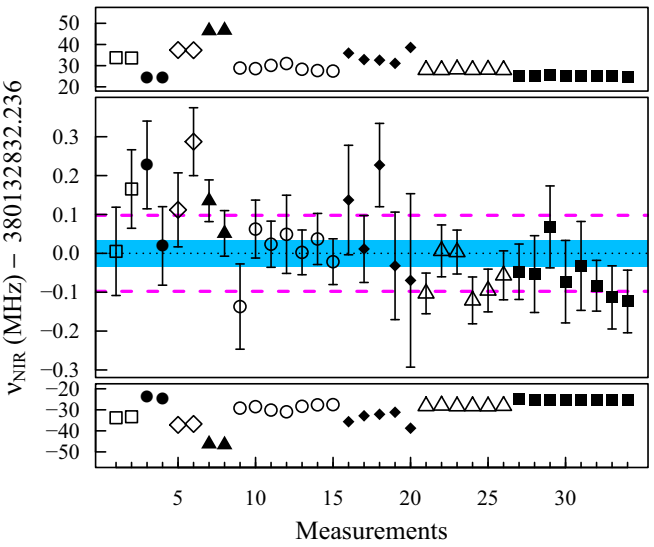

FIG. 5. Measured frequencies ν_{NIR} for the $50f0_3 \leftarrow GK(0,2)$ transition. The lower (upper) panel contains the measured frequencies $\nu_{NIR,a}$ ($\nu_{NIR,b}$). The mean values of pairs of measurements are displayed in the middle panel, where the vertical bars indicate one standard deviation. The standard deviation of the entire measurement set is indicated by the dashed magenta lines and the standard deviation of the mean of the different measurements by the cyan area. The different symbols indicate measurements taken on different days after full realignment of the laser and molecular beams.

the fit parameters were obtained using the robust covariance-matrix estimator [27]. The parameters obtained from the fit presented in Fig. 4 are listed in the inset.

Figure 5 presents the results of 34 measurements of the $50f0_3 \leftarrow GK(0,2)$ transition. The transition was recorded in eight series of measurements carried out on eight different days after full realignment of the laser and molecular beams. The top and bottom panels indicate the fitted line positions of the two Doppler components with frequencies $\nu_{NIR,a}$ and $\nu_{NIR,b}$ and the middle panel contains the corresponding central Doppler-free line position $\nu_{NIR} = (\nu_{NIR,a} + \nu_{NIR,b})/2$. Whereas the Doppler shifts of the lines measured on different days are different, the central frequency remains unchanged within the experimental uncertainty. Figure 5 thus illustrates that changing the alignment changes the two Doppler-shifted frequencies without affecting their average, as expected. The uncertainties $\sigma_{\nu_{NIR,a/b}}$ of the fitted line positions are between 50 and 220 kHz and can not be seen on the scale in Fig. 5. The estimator for the standard deviation of the entire data set is $\sigma_{stat,\,sample} = 98$ kHz and is indicated by dashed lines in Fig. 5. The comparison of $\sigma_{stat,\,sample}$ with the scatter of the individual line positions and their uncertainties validates our procedure of propagating the uncertainties. The final transition frequency, determined as the weighted mean of the 34 values presented in Fig. 5, is 12 679.866 424 0(12) cm^{-1} or 380 132 832.236(35) MHz. The statistical uncertainty of the mean frequency is estimated by $\sigma_{stat,\,sample}/\sqrt{8}$ to be 35 kHz, rather than by $\sigma_{stat,\,sample}/\sqrt{34} = 17$ kHz to account for the fact that the different measurements carried out on a given day might not be strictly independent, although the data in Fig. 5 do not reveal any obvious dependencies beyond those expected from the known day-to-day fluctuations of the experimental conditions, which are taken into account in the error budget.

B. Systematic uncertainties

To estimate systematic uncertainties, the experimental parameters (pressure, beam velocity, laser intensity, electric fields, ...) were varied and measurements were carried out for different values of the principal quantum number. The following sources of systematic uncertainties were considered.

Pressure shift. The pressure shift of high-n Rydberg states results from the scattering of the slow Rydberg electron off neutral molecules located within the Rydberg orbit [28–30]. Amaldi and Segré observed a blue-shift of the spectral positions of Rydberg states of 4.80 cm^{-1}/amagat in a gas cell filled with pure molecular hydrogen [28], which corresponds to 5.36 kHz/(10^{12} particles/cm^3). For the spectra used in the analysis, we estimated the H_2 molecule density in the beam at the excitation spot to be about 10^{11} particles/cm^3 and the pressure shift to be about 0.5 kHz, i.e., negligible.

The determination of particle densities in pulsed molecular-beam experiments is not trivial. To experimentally verify our estimate of the density, we (i) varied the stagnation pressure of the H_2 valve in the range from 0.5 to 6 bar, (ii) carried out measurements at valve temperatures of 298, 88, and 40 K, and (iii) measured spectra at different temporal positions within the gas pulse. In none of these experiments could we detect any shift within the precision limit of about 50 kHz of the measurements. It turned out that the skimmers we used to collimate the beam had a significant impact on the linewidths because of the tendency of intense beams to clog the skimmer orifice, causing a second expansion and a broadening of the velocity distribution in the transverse directions. This effect also reduced the density on the beam axis, preventing a quantitative analysis of the pressure shift. The largest effect we could notice is a broadening of the lines in spectra recorded in the middle of the gas pulse at high stagnation pressure. We attribute this effect to the collisional heating of the beam at the second skimmer, which results in a reduced density and an enhanced collision rate in the measurement region. Depending on the expansion conditions, we observed Gaussian or Lorentzian line shapes.

The narrowest lines were measured at stagnation pressures of less than 2 bar and in the early part of the gas pulse. The spectra used for the analysis (see Fig. 4) were all taken under conditions where the line profiles were Lorentzian, with linewidths in the range between 5 and 7 MHz. Because no pressure shift was observed, but only a broadening, the effects of the expansion conditions and the pressure are accounted for by the statistical uncertainties discussed in the previous section.

Doppler shift. Our procedure to cancel the first-order Doppler shift consisted of overlapping the laser beam and its reflection at a distance of 12 m from the reflection mirror. The maximal error in the determination of the line centers of the two Doppler components is given by the maximal deviation from exact 180° reflection. We estimate this deviation to be at most 0.003°, which results in a systematic error of 110 kHz at 88 K and 12 680 cm^{-1}. Because our procedure to determine line centers involved measuring each line several times after realigning the NIR laser and its back reflection and averaging

the results, we expect a systematic shift from the first-order Doppler effect to average out over the entire data set (see Fig. 5) and thus to only contribute to the statistical uncertainty.

The second-order Doppler effect induces a red-shift of $\nu_{\rm NIR} v_{\rm beam}^2/(2c^2)$ and can be calculated from the speed of the beam $v_{\rm beam}$ (c is the speed of light). At the excitation wave number of 12 680 cm^{-1} and for nozzle temperatures of 298 K [$v_{\rm beam} = 2659(81)$ m/s] and 88 K [$v_{\rm beam} = 1389(22)$ m/s] we obtain shifts of 15.0(9) and 4.1(5) kHz, respectively. The line centers were corrected for this effect although the second-order Doppler shift is much less than the precision of our measurements.

dc Stark shift. Residual stray electric fields $\vec{F}$ can mix states with $\Delta l = \pm 1$ and cause a shift of the line positions that originates almost exclusively from the quadratic Stark effect

$$\Delta E_{\rm dc\ Stark} = -\tfrac{1}{2}\alpha_n \left(F_x^2 + F_y^2 + F_z^2\right) \quad (4)$$

of the nf Rydberg states investigated, where α_n is the polarizability of the nf Rydberg states. To minimize systematic Stark shifts, we compensated the stray field following the procedure described in Ref. [31] in all three dimensions with the electrode configuration described in Sec. II (see Fig. 3). The quadratic Stark shifts measured for specifically applied fields also allowed us to determine the polarizabilities of the Rydberg states, i.e., $5.47(11) \times 10^4$ MHz/(V/cm)^2 and $5.3(3) \times 10^5$ MHz/(V/cm)^2 for the $50f0_3$ and $70f0_3$ Rydberg states, respectively. These polarizabilities are large and conform to the expected n^7 scaling law [32]. From these measurements and a measurement of the transition to the $200f0_3$ level (not shown), we expect the residual stray fields to be less than 800 μV/cm, which would cause systematic shifts of the $50f0_3$ and $70f0_3$ levels of 18 and 170 kHz, respectively. The effect of inhomogeneous stray fields caused by ions generated in the excitation volume by resonance-enhanced multiphoton ionization via the $GK(0,2)$ state was examined by varying the pulse energy of the VIS laser. It was found to be negligible at $n = 50$ for pulse energies below 10 μJ, corresponding to the production of at most five ions per experimental cycle.

ac Stark shift. To estimate the ac Stark shifts induced by the NIR-laser field, we varied the NIR-laser power from 12 to 900 mW while keeping the beam size at the excitation spot constant. Because the laser beam at the excitation spot had a beam waist radius of about 0.5 mm we could not observe any shift within the precision of our measurements. A possible ac Stark shift of the transition frequency can be estimated from the ponderomotive shift of the Rydberg electron according to

$$\Delta E_{\rm ac\ Stark} = \frac{e^2 I_{\rm NIR}}{8c\epsilon_0 m_e \pi^2 \nu_{\rm NIR}^2}. \quad (5)$$

At a maximal peak intensity of $I_{\rm NIR} \sim 2.5 \times 10^6$ W/m^2 (corresponding to a Gaussian beam with 1 W and 0.5 mm beam waist) the ponderomotive shift is 3.6 kHz. Typical measurements were carried out at lower laser powers so that the ponderomotive shift is entirely negligible. Shifts caused by the polarizability of the intermediate GK state and the ionic H_2^+ core in the NIR-light field are estimated to be smaller than 60 Hz.

Zeeman shift. The magnetic field inside the mumetal shield was measured using a Hall magnetic probe to be less than 40 mG, limited by the sensitivity of the gauge. The orbital angular momentum l of molecular Rydberg states with high principal quantum number is uncoupled from the internuclear axis and the Zeeman splitting of singlet states is comparable to the Zeeman splitting of atomic Rydberg states. The Rydberg states studied in this work have pure singlet character because of the absence of hyperfine and spin-rotation interactions in the $N^+ = 0$ ionic state. The estimated splitting between the $m_l = \pm 3$ sublevels of the f Rydberg states is 300 kHz in a field of 40 mG. Because we do not select a specific Zeeman sublevel, this effect should only lead to a broadening of the lines but not to a shift of the transition frequencies. A shift would only result from an asymmetry in the excitation of $\Delta m_l = \pm 1$ transitions resulting from a deviation from linear polarization. Our lasers are very close to being purely linearly polarized and the short lifetimes of the intermediate states in combination with our experimental conditions (small number of scattered VUV and VIS photons) prevent optical pumping into one Zeeman component. A magnetic field could also cause a shift through the motional Stark effect, which can cause a maximum electric field $F = v_{\rm beam} B$ of 120 μV/cm and 65 μV/cm for supersonic expansions generated by pulsed valves held at 298 and 88 K, respectively, which is much less than the residual dc electric field. In an effort to quantify a possible Zeeman shift caused by the residual magnetic field, spectra of the $51f0_3 \leftarrow 49d0_2$ transition of H_2 were measured using optical-optical-millimeter-wave triple-resonance spectroscopy as described in Ref. [33]. After compensating electric stray fields, the width of the transition was only 270 kHz, limited by the inhomogeneity of the electric fields (after compensation) over the ~5-mm-long path the molecules traversed during the interaction time. No indication of Zeeman broadening could be detected in these measurements, from which we conclude that the residual magnetic field in the magnetically shielded excitation volume is much less than the 40-mG detection limit of our Hall magnetic probe. We conservatively take an uncertainty of 10 kHz for a possible Zeeman shift caused by the residual magnetic field.

Line-shape model. Because our line-shape model is not based on an exact analysis of all geometrical constraints, including those associated with the velocity distribution, we have included a systematic uncertainty of 50 kHz, which corresponds to a hundredth of the measured full width at half maximum.

The uncertainties of the transition to the $70f0_3$ Rydberg state were estimated in the same manner. The only significant difference compared to the transition to the $50f0_3$ state arises from the larger polarizability of the $70f0_3$ level, which leads to larger statistical and systematic uncertainties. The systematic uncertainty results from the residual stray electric field, which gives rise to a red-shift of the transition frequency. The statistical uncertainty is given by the accuracy with which the daily electric field compensation was carried out.

The positions of the $50f0_3$ and $70f0_3$ levels with respect to the $GK(0,2)$ state were measured to be

$$\nu_{50f,GK} = 380\,132\,832.236(0.035)_{\rm stat}(0.054)_{\rm sys}{\rm MHz} \quad (6)$$

and

$$\nu_{70f,GK} = 380\,777\,345.01(0.07)_{\rm stat}(0.18)_{\rm sys}{\rm MHz}, \quad (7)$$

respectively, which represent the main result of the present investigation.

IV. DISCUSSION AND CONCLUSIONS

The results presented in the previous section demonstrate that transitions to Rydberg states of molecular hydrogen can be measured from the $GK(0,2)$ level with a relative accuracy $\Delta\nu/\nu$ of 2×10^{-10} and an absolute accuracy of 65 kHz in the case of the $50f0_3$ level. This corresponds to an improvement by a factor of more than 10 over the previous measurements using pulsed NIR radiation [12]. This improvement primarily resulted from the suppression of the ac Stark shift and the frequency chirp in the experiments presented here.

In the context of a precision measurement of the ionization energy of H_2 following the scheme presented in Eq. (2) one should emphasize that similar measurements of $\mathcal{N}$ different members of a given Rydberg series will improve the ionization energy by a factor of $\sqrt{\mathcal{N}}$. Consequently, only a few such measurements would in principle suffice to reach the accuracy of 42 kHz needed to make a contribution to the determination of the proton charge radius. Ideally, these measurements should include well-spaced Rydberg levels to guarantee a reliable extrapolation of the Rydberg series, which can be performed with an accuracy of better than 100 kHz [10]. At present, stray electric fields still represent a difficulty beyond $n = 70$ for f levels. An improvement of more than two orders of magnitude of the ionization energy over the results of Liu *et. al.* [11] can be anticipated once the accuracy of the $X-GK$ interval has been improved. A measurement of the $X-GK$ interval with high accuracy by two-photon Doppler-free spectroscopy following a similar scheme as that employed in the recent determination of the $X-EF$ interval [9] should be possible in future.

We conclude this article by a short comparison with a recent determination of optical transition frequencies to high-n Rydberg states of Cs [14]. The measurements relied on the determination of the frequencies of one-photon transitions from the $6\,^2S_{1/2}$ ground state to the $n\,^2P_J$ Rydberg states of ^{133}Cs with n in the range from 27 to 74 using a narrow-band cw UV-laser system referenced to a frequency comb as described in Sec. II. The measurement was performed with samples of ultracold atoms ($T = 70\ \mu$K) prepared by laser cooling in a magneto-optical trap and released from an optical dipole trap.

The results of this comparison are presented in Table I, which contains the main physical properties of the systems relevant for the determination of the ionization energy. We refer to Ref. [14] for the discussion of the systematic and statistical uncertainties of the Cs measurement. The main differences between the two measurements result from (i) the reduction of all effects related to the speed of the atoms (Doppler effect) in the Cs experiment, (ii) the fact that the initial states in Cs is the ground state, which suppresses natural broadening, and (iii) the presence of surfaces close to the atom sample in the magneto-optical trap (MOT), which enhances the electric-field inhomogeneities and forces one to strongly reduce the experimental volume to 3.4×10^{-3} mm^3 in the Cs experiment compared to about 1 mm^3 in the H_2 experiment. Because the particle densities in both experiments are similar, this measure leads to a much weaker signal in the Cs experiment, which in turn necessitates longer acquisition times to achieve a comparable signal-to-noise ratio.

For the comparison, the transition to the $74p\,^2P_{3/2}$ level of Cs was chosen because this state has a similar polarizability as the $50f0_3$ Rydberg state of H_2. The dominant sources of systematic uncertainties originate from the ac and dc Stark effects in the Cs experiment and from the Zeeman and dc Stark effects, the Doppler effect, and the incomplete line-shape model in the H_2 experiments. The comparison (summarized in Table I) reveals that the experimental approach reported in this article for measurements in a molecular beam of H_2 yields statistical and systematic uncertainties that are only slightly larger than those that can be achieved with ultracold samples of alkali-metal atoms.

The position of high Rydberg states of H_2 can now be measured in the optical domain with an accuracy comparable to that achieved in earlier studies using Rydberg-Rydberg transitions in the far-infrared [34] and millimeter-wave [33] regions. The measurement of Rydberg-Rydberg transitions at low frequencies is well suited to determine the rotational, fine, and hyperfine intervals in molecular ions, but it is not suitable for the determination of vibrational intervals in the ion because of restrictions imposed by the Franck-Condon principle. Optical transitions from low-n intermediate states or from valence states, which have Born-Oppenheimer potential functions that differ from the potential function of the ion, allow access to Rydberg series converging on a very broad range of rovibronic levels of the molecular hydrogen ion [35–37], offering the prospect of measuring a wide range of rovibrational energy intervals of this ion.

The results presented in this article demonstrate that precision optical spectroscopy of high molecular Rydberg states in supersonic beams represents a powerful method for the determination of ionization energies and of rovibronic intervals of molecular ions. The accuracy reached in this work compares favorably with that achieved in the best measurements of energy intervals in molecular ions using ion traps [38].

ACKNOWLEDGMENT

This work was supported financially by the Swiss National Science Foundation (Project No. 200020-172620) and the European Research Council (ERC) under the European Union's Horizon 2020 research and innovation programme (Advanced Grant No. 743121).

[1] K. Piszczatowski, G. Łach, M. Przybytek, J. Komasa, K. Pachucki, and B. Jeziorski, J. Chem. Theory Comput. **5**, 3039 (2009).

[2] M. Puchalski, J. Komasa, P. Czachorowski, and K. Pachucki, Phys. Rev. Lett. **117**, 263002 (2016).

[3] M. Puchalski, J. Komasa, and K. Pachucki, Phys. Rev. A **95**, 052506 (2017).

[4] J.-P. Karr, L. Hilico, J. C. J. Koelemeij, and V. I. Korobov, Phys. Rev. A **94**, 050501 (2016).

[5] V. I. Korobov, L. Hilico, and J.-P. Karr, Phys. Rev. Lett. **118**, 233001 (2017).
[6] R. J. Hill, EPJ Web of Conferences **137**, 01023 (2017).
[7] A. Beyer, L. Maisenbacher, A. Matveev, R. Pohl, K. Khabarova, A. Grinin, T. Lamour, D. C. Yost, T. W. Hänsch, N. Kolachevsky, and T. Udem, Science **358**, 79 (2017).
[8] P. J. Mohr, D. B. Newell, and B. N. Taylor, Rev. Mod. Phys. **88**, 035009 (2016).
[9] R. K. Altmann, L. Dreissen, E. J. Salumbides, W. Ubachs, and K. S. E. Eikema (unpublished).
[10] D. Sprecher, Ch. Jungen, W. Ubachs, and F. Merkt, Faraday Discuss. **150**, 51 (2011).
[11] J. Liu, E. J. Salumbides, U. Hollenstein, J. C. J. Koelemeij, K. S. E. Eikema, W. Ubachs, and F. Merkt, J. Chem. Phys. **130**, 174306 (2009).
[12] D. Sprecher, M. Beyer, and F. Merkt, Mol. Phys. **111**, 2100 (2013).
[13] S. A. Astashkevich and B. P. Lavrov, J. Phys. Chem. Ref. Data **44**, 023105 (2015).
[14] J. Deiglmayr, H. Herburger, H. Saßmannshausen, P. Jansen, H. Schmutz, and F. Merkt, Phys. Rev. A **93**, 013424 (2016).
[15] D. Bailly, E. J. Salumbides, M. Vervloet, and W. Ubachs, Mol. Phys. **108**, 827 (2010).
[16] Device information Coherent, 899-29.
[17] Device information Coherent, Verdi.
[18] Device information Menlo Systems, FC1500-250-WG.
[19] G. Ritt, G. Cennini, C. Geckeler, and M. Weitz, Appl. Phys. B **79**, 363 (2004).
[20] D. Haubrich and R. Wynands, Opt. Commun. **123**, 558 (1996).
[21] Device information HighFinesse, WS-7.
[22] Device information Stanford Research Systems, FS725.
[23] Device information Spectrum Instruments, TM-4.
[24] P. Allmendinger, J. Deiglmayr, O. Schullian, K. Höveler, J. A. Agner, H. Schmutz, and F. Merkt, Chem. Phys. Chem. **17**, 3596 (2016).
[25] Device information Vacoflux, 50.
[26] H. Naus, I. H. M. v. Stokkum, W. Hogervorst, and W. Ubachs, Appl. Opt. **40**, 4416 (2001).
[27] R. Carroll and D. Ruppert, *CRC Monographs on Statistics and Applied Probability* (Taylor and Francis, London, 1988)
[28] E. Amaldi and E. Segrè, Il Nuovo Cimento (1924-1942) **11**, 145 (1934).
[29] E. Fermi, Il Nuovo Cimento (1924-1942) **11**, 157 (1934).
[30] G. Herzberg and C. Jungen, J. Mol. Spectrosc. **41**, 425 (1972).
[31] A. Osterwalder and F. Merkt, Phys. Rev. Lett. **82**, 1831 (1999).
[32] T. F. Gallagher, *Rydberg Atoms* (Cambridge University Press, Cambridge, 1994).
[33] A. Osterwalder, A. Wüest, F. Merkt, and Ch. Jungen, J. Chem. Phys. **121**, 11810 (2004).
[34] C. Haase, M. Beyer, C. Jungen, and F. Merkt, J. Chem. Phys. **142**, 064310 (2015).
[35] M. Beyer and F. Merkt, Phys. Rev. Lett. **116**, 093001 (2016).
[36] M. Beyer and F. Merkt, J. Mol. Spectrosc., **330**, 147 (2016).
[37] M. Beyer and F. Merkt, J. Phys. B: At., Mol. Opt. Phys. **50**, 154005 (2017).
[38] J. Biesheuvel, J.-P. Karr, L. Hilico, K. S. E. Eikema, W. Ubachs, and J. C. J. Koelemeij, Nat. Commun. **7**, 10385 (2016).
[39] M. L. Zimmerman, M. G. Littman, M. M. Kash, and D. Kleppner, Phys. Rev. A **20**, 2251 (1979).